J Neurophysiol 96: 1517–1529, 2006.
First published June 7, 2006; doi:10.1152/jn.01212.2005.

Membrane Resting Potential of Thalamocortical Relay Neurons Is Shaped by the Interaction Among TASK3 and HCN2 Channels

Sven G. Meuth,[1,*] Tatyana Kanyshkova,[6,*] Patrick Meuth,[6,*] Peter Landgraf,[2] Thomas Munsch,[3] Andreas Ludwig,[4] Franz Hofmann,[5] Hans-Christian Pape,[6] and Thomas Budde[7]

[1]*Neurologische Klinik, Bayerische Julius-Maximilians-Universität, Würzburg;* [2]*Leibniz Institut für Neurobiologie, Magdeburg;* [3]*Institut für Physiologie, Otto-von-Guericke-Universität, Magdeburg;* [4]*Institut für Experimentelle und Klinische Pharmakologie und Toxikologie, Uni Erlangen-Nürnberg, Erlangen;* [5]*Institut für Pharmakologie und Toxikologie, Technische Universität, München; and* [6]*Institut für Physiologie I and* [7]*Institut für Experimentelle Epilepsieforschung, Westfälische Wilhelms-Universität, Münster, Germany*

Submitted 16 November 2005; accepted in final form 1 June 2006

Meuth, Sven G., Tatyana Kanyshkova, Patrick Meuth, Peter Landgraf, Thomas Munsch, Andreas Ludwig, Franz Hofmann, Hans-Christian Pape, and Thomas Budde. Membrane resting potential of thalamocortical relay neurons is shaped by the interaction among TASK3 and HCN2 channels. *J Neurophysiol* 96: 1517–1529, 2006. First published June 7, 2006; doi:10.1152/jn.01212.2005. By combining molecular biological, electrophysiological, immunological, and computer modeling techniques, we here demonstrate a counterbalancing contribution of TASK channels, underlying hyperpolarizing K^+ leak currents, and HCN channels, underlying depolarizing I_h, to the resting membrane potential of thalamocortical relay (TC) neurons. RT-PCR experiments revealed the expression of TASK1, TASK3, and HCN1–4. Quantitative determination of mRNA expression levels and immunocytochemical staining demonstrated that TASK3 and HCN2 channels represent the dominant thalamic isoforms and are coexpressed in TC neurons. Extracellular acidification, a standard procedure to inhibit TASK channels, blocked a TASK current masked by additional action on HCN channels. Only in the presence of the HCN blocker ZD7288 was the pH-sensitive component typical for a TASK current, i.e., outward rectification and current reversal at the K^+ equilibrium potential. In a similar way extracellular acidification was able to shift the activity pattern of TC neurons from burst to tonic firing only during block of I_h or genetic knock out of HCN channels. A single compartmental computer model of TC neurons simulated the counterbalancing influence of TASK and HCN on the resting membrane potential. It is concluded that TASK3 and HCN2 channels stabilize the membrane potential by a mutual functional interaction, that the most efficient way to regulate the membrane potential of TC neurons is the converse modulation of TASK and HCN channels, and that TC neurons are potentially more resistant to insults accompanied by extracellular pH shifts in comparison to other CNS regions.

INTRODUCTION

Despite its fundamental importance, rather little is known about the ionic conductances underlying the resting membrane potential of central neurons. In general, the resting potential is assumed to be determined by channels active below firing threshold, with I_h (Pape 1996) and $I_{K\text{-leak}}$ (Jones 1989) playing major roles. Modulation of currents active below threshold is of particular interest because neuronal excitability is regulated in this manner. Recently the molecular nature of I_h and $I_{K\text{-leak}}$ was illuminated by the cloning of four members of the HCN channel family giving rise to native I_h currents in neurons and heart cells (Craven and Zagotta 2006) and five members of the TASK channel family, typically giving rise to highly regulated time- and voltage-independent K^+ background currents (Patel and Lazdunski 2004). Depending on their sensitivity to changes in extracellular pH and based on sequence homologies TASK1, TASK3, and TASK5 channels constitute one subclass (Lesage 2003). Despite this progress in understanding, the molecular constituents and functional interaction of $I_{K\text{-leak}}$ and I_h in specific cell types are yet not well understood.

Thalamocortical relay (TC) neurons offer a model system to gain our understanding of membrane currents that constitute the resting membrane potential for the following reasons. *1*) TC neurons display large state-dependent shifts in membrane potential that are associated with a change from rhythmic burst firing at hyperpolarized potentials during slow-wave sleep to tonic single-spike activity at depolarized potentials during wakefulness (Steriade et al. 1997). Most important, the depolarization-induced cessation of burst activity depends on the downregulation of $I_{K\text{-leak}}$ and the upregulation of I_h by a number of transmitters of the ascending arousal system of the brain stem (McCormick 1992). Because of their important function as targets of multiple regulatory pathways, $I_{K\text{-leak}}$ and I_h are in the main focus of the present study. *2*) Previous studies have begun to unravel the functional roles of HCN and TASK channels in TC neurons. Although it was shown that inhibition of TASK1 and TASK3 channels depolarize TC neurons, thereby preferring tonic single spike activity (Meuth et al. 2003, 2006), the genetic knock out or block of the HCN2 channels hyperpolarizes TC neurons, thereby preferring burst firing (Ludwig et al. 2003). *3*) The pH dependency of HCN (Zong et al. 2001) and TASK (Rajan et al. 2000) channels and their corresponding membrane currents (Meuth et al. 2003; Munsch and Pape 1999) offer an experimental tool to probe this mutual functional interaction. Therefore we used extracellular acidification, molecular biological, electrophysiological, and computer modeling techniques to demonstrate the contri-

* S. G. Meuth, T. Kanyshkova, and P. Meuth contributed equally to this work.

Address for reprint requests and other correspondence: T. Budde, Westfälische Wilhelms-Universität, Medizinische Fakultät, Institut für Experimentelle Epilepsieforschung, Hüfferstr. 68, D-48149 Münster, Germany (E-mail: tbudde@uni-muenster.de).

The costs of publication of this article were defrayed in part by the payment of page charges. The article must therefore be hereby marked "*advertisement*" in accordance with 18 U.S.C. Section 1734 solely to indicate this fact.

bution of HCN2 and TASK3/TASK1 channels to the regulation of the resting membrane potential in TC neurons.

METHODS

Preparation

Rats and mice (postnatal days 12–-29) were anesthetized with halothane, decapitated, and used for electrophysiological, immunohistochemical, and molecular biological analysis. A block of tissue containing the thalamus was removed and placed in ice-cold saline, containing (in mM): Sucrose, 200; PIPES, 20; KCl, 2.5; NaH_2PO_4, 1.25; $MgSO_4$, 10; $CaCl_2$, 0.5; and dextrose, 10; pH 7.35 with NaOH. Thalamic slices were prepared as coronal sections on a vibratome. Before recording, slices were kept submerged in standard artificial cerebrospinal fluid (ACSF) containing (in mM): NaCl, 125; KCl, 2.5; NaH_2PO_4, 1.25; $NaHCO_3$, 24; $MgSO_4$, 2; $CaCl_2$, 2; and dextrose, 10; pH adjusted to 7.35 by bubbling with a mixture of 95% O_2-5% CO_2.

Whole cell patch-clamp recordings

Recordings were performed on visually identified TC neurons of the dorsal lateral geniculate nucleus (dLGN) at room temperature. Slices were recorded in a solution containing (in mM): NaCl, 120; KCl, 2.5; NaH_2PO_4, 1.25; HEPES, 30; $MgSO_4$, 2; $CaCl_2$, 2; and dextrose, 10; pH 7.3 or 6.3 was adjusted with HCl. Electrical activity was measured with pipettes pulled from borosilicate glass (GC150T-10, Clark Electromedical Instruments, Pangbourne, UK), connected to an EPC-10 amplifier (HEKA Elektronik, Lamprecht, Germany), and filled with (in mM): K-gluconate, 95; K_3-citrate, 20; NaCl, 10; HEPES, 10; $MgCl_2$, 1; Ca Cl_2, 0.5; BAPTA, 3; Mg-ATP, 3; and Na-GTP, 0.5. The internal solution was set to a pH of 7.25 with KOH and an osmolality of 295 mOsm/kg. Typical electrode resistance was 2–3 MΩ, with an access resistance in the range of 5–15 MΩ. Series resistance compensation of >40% was routinely used. Electrophysiological experiments were governed by Pulse software (HEKA Elektronik) operating on an IBM-compatible PC. A liquid junction potential of 8 ± 1 mV (n = 6) was taken into account.

I_h was activated using hyperpolarizing voltage steps from a holding potential of −43 to −133 mV in 10-mV increments. To increase stability of whole cell recordings the pulse length was decreased by 1,500 ms with increasing depth of the hyperpolarization (3.5-s pulse length at −130 mV). Steady-state activation of I_h activation, p(V), was estimated by normalizing the tail current amplitudes (I), 50 ms after stepping to a constant potential from a variable amplitude step using the following equation

$$p(V) = (I - I_{min})/(I_{max} - I_{min})$$

where I_{max} is the tail current amplitude for the voltage step from −133 to −98 mV and I_{min} is the voltage step from −43 to −98 mV, respectively. I_h activation was usually well accounted for a Boltzmann distribution of the following form

$$p(V) = 1/\{1 + \exp[(V - V_h)/k]\}$$

where V_h is the voltage of half-maximal activation and k is the slope factor.

During current-clamp recordings the instantaneous frequency (f) of action potential generation was determined by analyzing the first two action potentials elicited by a depolarizing current pulse.

All results are presented as means ± SE. Substance effects were tested for statistical significance using the nonparametric Mann–Whitney test. Where applicable (Gaussian distribution of measured values), a parametric t-test modified for small samples was used. Differences were considered statistically significant at $P < 0.05$.

Drugs

ZD7288 [4-(*N*-ethyl-*N*-phenylamino)-1,2-dimethyl-6-(methylamino) pyridinium chloride; Biotrend, Cologne, Germany] was directly dissolved in the external recording solution.

Computer simulations with NEURON

For computer simulations, a previously described single-compartment TC neuron model (Huguenard and McCormick 1992; McCormick and Huguenard 1992) was adapted to NEURON (Hines and Carnevale 2001; Meuth et al. 2005). The model is based on the mathematical description of I_A, I_{K2}, I_C, I_L, I_T, I_{NaP}, and I_h and displays the two typical modes of action potential generation in thalamic cells: burst firing with two to six action potentials riding on a low-threshold Ca^{2+} spike (LTS) and single-spike activity with tonic trains of action potentials. This well-established model was extended by incorporating the inward rectifying current I_{Kir} of the Hodgkin–Huxley form (Williams et al. 1997) and the background potassium current I_{TASK}. The general equation describing the membrane potential over the time is

$$C_m(dV/dt) = -(I_{leak} + I_{TASK} + I_{Kir} + I_h) + I_{inject}$$

where C_m is the membrane capacitance and I_{inject} is the injection current. The noninactivating current I_{Kir} was modeled as previously described (Williams et al. 1997)

$$I_{Kir} = g_{Kir}m^a(V - E_{Kir})$$

where g_{Kir} is the maximal conductance of the current I_{Kir}, whereas m is the activation variable, and a is its exponent (=3). E_{Kir} is the reversal potential of the current I_{Kir}. The outwardly rectifying pH-sensitive leak current I_{TASK} was modeled as a mathematical fit through the currents measured in the current publication

$$I_{TASK} = g_{TASK}m(V - E_{TASK})$$

where g_{TASK} is the maximal conductance of the current I_{TASK}, whereas the driving force is defined as reversal potential E_{TASK} subtracted from the membrane potential V. The activation variable m is defined as

$$m = y_0 + A_1e^{(x/t_1)}/(V - E_{TASK})$$

All values were assumed for maximal conductances and fixed reversal potentials and were systematically varied in some simulations. To demonstrate the contribution of the leak potassium current I_{TASK} to the total leak of TC neurons, we calculated a pH-insensitive (g_{leak}) and a pH-sensitive leak (g_{TASK}) conductance, respectively. The proportion of both leaks was changed systematically to achieve a model that simulates the pH effect in rat TC neurons. All computer modeling was carried out at 35°C.

The magnitude of pH-dependent effects on TASK (90% reduction) and HCN (25% reduction) channels used in computer modeling were estimated from previously published data. The reduction of I_h resulting from an intracellular shift of 0.8 pH units is roughly 25% (Munsch and Pape 1999). Both, TASK1 and TASK3 channels are inhibited by acidification, although over different pH ranges (pK values ≈7.5 and ≈6.7 for TASK1 and TASK3, respectively) (Duprat et al. 1997; Kim et al. 2000; Rajan et al. 2000). Tandem-linked heterodimeric TASK channel constructs displayed pH sensitivity (pK ≈ 7.3) closer to that of TASK1 than to TASK3 (Berg et al. 2004; Czirjak and Enyedi 2002). Therefore TASK1 and TASK3 channels reveal 95 and 75% inhibition at pH 6.4, respectively, and an intermediate value of 90% was used for modeling.

Preparation of dissociated cell cultures from the dorsal thalamus

Dorsal thalami were prepared from embryos (Long–Evans rats) at stage E 19 and subsequently transferred into ice-cold Hanks balanced

salt solution (HBSS, without Ca/Mg). After triple washing with 5 ml HBSS each, 2.0 ml HBSS, containing 0.5% trypsin, was added to the tissue, followed by incubation at 37°C for 20 min. Tissue was washed again five times with 5 ml HBSS each and finally transferred into 2-ml tubes with HBSS, containing 0.01% DNAseI. To dissociate thalamic tissue, it was pressed slowly three times through a 0.9-mm-gauge needle followed by three passages through a 0.45-mm-gauge needle. The remaining cell suspension was poured through a nylon tissue (mesh aperture 125 μm) into a 50-ml tube and filled up with 18 ml Dulbecco's modified Eagle medium (DMEM; Gibco, Eggenstein, Germany). After estimating cell quantity, the suspension was diluted with DMEM in accordance to the required density of 16,000 cells/ml. A 500-μl aliquot of this suspension was placed on each well of a 24-well plate, containing defatted, baked, and poly-D-lysine–coated coverslips. The cell cultures were incubated at 37.0°C and 5% CO_2 up to the appropriate time points and finally fixed with 4% perfluoroalkoxy polymer resin (PFA) for 10 min.

Immunochemistry

After 21 days in vitro (DIV 21) PFA-fixed cells were washed three times with 10 mM PBS and subsequently preincubated at 4°C in blocking solution [10 mM PBS, 10% horse normal serum (NHS), 2% bovine serum albumin (BSA), 5% sucrose, 0.3% Triton X-100]. After 1 h, primary antibodies (rabbit anti-HCN2, 1:500, Alomone Labs, Jerusalem, Israel; goat anti-TASK3, 1:300, Santa Cruz Biotechnology, Heidelberg, Germany; rabbit anti-parvalbumin, 1:500, Swant, Bellinzona, Switzerland; mouse anti-MAP2 1:1,000, Sigma, Deisenhofen, Germany) were added to the blocking solution and incubated overnight. Thereafter cultures were washed with 10 mM PBS including 0.3% Triton X-100 and incubated with secondary antibodies (Cy5-conjugated rabbit-anti-mouse IgG, 1:1,000, Sigma; Cy3-conjugated goat-anti-rabbit IgG, 1:1,000; Dianova, Hamburg, Germany, Alexa-Fluor-488 conjugated donkey-anti-goat, 1:1,000; Molecular Probes; in blocking solution) for 2 h, washed, and coverslipped with Moviol. Omission of primary and secondary antibodies resulted in lack of fluorescent signals.

Reverse transcription–polymerase chain reaction (RT-PCR) assays

Poly(A) mRNA was prepared from freshly dissected tissue by extraction with Trizol reagent according to the manufacturer's instructions (Oligotex, Qiagen, Hilden, Germany). First-strand cDNA was primed with oligo(dT) from 0.5–1 μg of mRNA and synthesized using the SuperScript II enzyme (Invitrogen Life Technologies) at 42°C for 50 min. PCR was performed in a 30-μl reaction mixture using 0.75 U *Taq* polymerase (Qiagen) for HCN templates or 0.75 U HotStar*Taq* polymerase (Qiagen) for amplification of TASK templates; mixture in both cases contained 1.5 mM $MgCl_2$, 0.2 mM of each dNTP, and 50 pmol of each primer. Cycling protocols were: 3 min at 94°C, 35 cycles: 30 s at 94°C, 1 min at 58°C, 1 min at 72°C, 7 min at 72°C for HCNs; and 15 min at 95°C, 35 cycles: 30 s at 94°C, 1 min at 58°C, 1 min at 72°C, 10 min at 72°C for TASK amplification. The following primers were used

HCN1 (nucleotides 1462–1750) Accession No. AF247450

forward: CTC TCT TTG CTA ACG CGG AT
reverse: TTG AAA TTG TCC ACC GAA

HCN2 (nucleotides 1059–1428) Accession No. AF247451

forward: GTG GAG CGA ACT CTA TTC GT
reverse: GTT CAC AAT CTC CTC ACG CA

HCN3 (nucleotides 1713–1945) Accession No. AF247452

forward: GCA GCA TTT GGT ACA ACA CG
reverse: AGC GTC TAG CAG ATC GAG C

HCN4 (nucleotides 1871–2042) Accession No. AF247453

forward: GCA GCG CAT CCA CGA CTA C
reverse: CGT CAC AAA GTT GGG GTC TGC

TASK1 (nucleotides 220–735) Accession No. AB048823

forward: CAC CGT CAT CAC CAC AAT CG
reverse: TGC TCT GCA TCA CGC TTC TC

TASK2 (nucleotides 330–959) Accession No. AF259395

forward: TGG GCG CCT CTT CTG TGT CTT CTA
reverse: TCC CCT CCC CCA CTT GTT TTC ATT

TASK3 (nucleotides 188–602) Accession No. AF192366

forward: ATG AGA TGC GCG AGG AGG AGA AAC
reverse: ACG AGG CCC ATG CAA GAA AAG AAG

TASK5 (nucleotides 137–700) Accession No. AF294353

forward: GAG CCT GGG CGA GCG TCT GAA C
reverse: CGG GCC CGG AGT CTG TCT GG

TREK1 (nucleotides 447–1119) Accession No. NM_172041

forward: ACA GAA CTT CAT AGC CCA GCA T
reverse: TCC CAC CTC TTC CTT CGT CT

TREK2 (nucleotides 1192–1639) Accession No. NM_023096

forward: CAG TGG GCT TTG GTG ATT TTG T
reverse: AGG CGT AGG TTA TTG GGT CTG TT

TRAAK (nucleotides 766–1143) Accession No. NM_053804

forward: AAC TGG TTG CGA GCG GTG TC
reverse: GGG CTT CTT CGT TGG GTT GG

THIK1 (nucleotides 404–805) Accession No. NM_022293

forward: CGT GGG CAC AGT GGT AAC TA
reverse: GCT CCA CAG GAG ATG GCT AC

THIK2 (nucleotides 764–1013) Accession No. NM_022292

forward: CCT TCC TCC GGC ACT ACG AG
reverse: ATG AAG GCC AGC AGC GAG AT

Multiplex and nested PCR in isolated neurons

mRNAs from 10 identified TC neurons were collected using the Dynabeads mRNA direct micro kit (Dynal, Oslo, Norway). First cDNA was primed with oligo$(dT)_{25}$, immobilized on the beads, and synthesized using the Sensiscript reverse transcriptase (Qiagen) at 37°C for 1 h.

After reverse transcription, the cDNAs for TASK3 and HCN2 were amplified simultaneously as a multiplex PCR. For the amplification of TASK3 the primers described above were used; for HCN2 (nucleotides 688–1652) the multiplex primers were as follows: forward, TAC CTG CGT ACG TGG TTC GT, reverse, AAA TAG GAG CCA TCT GAC A. First multiplex amplification was performed in 50 μl containing 50 pmol of each primer, 5 U Platinum *Taq* polymerase (Invitrogen) by using the following cycling program: 4 min at 95°C,

2 cycles: 30 s at 94°C, 1 min at 58°C, 5 min at 72°C, then cDNA library was removed and amplification proceeded with an additional 35 cycles: 30 s at 94°C, 1 min at 58°C, 1 min at 72°C, 7 min at 72°C. Nested amplification was carried out individually for each target in 50 μl reaction mix using 5 μl from the first amplification product, 10 pmol of correspondent primers, and 2.5 U Platinum *Taq* polymerase. Cycling protocol was: 4 min at 95°C, 30 cycles: 30 s at 94°C, 1 min at 58°C, 1 min at 72°C, 7 min at 72°C.

The efficiency of cDNA synthesis was controlled by single PCR amplification of glyceraldehyde-3-phosphate dehydrogenase (GAPDH) from the cDNA libraries using the primers mentioned above. PCR amplification was performed in 50 μl containing 10 pmol of each primer, 2.5 U Platinum *Taq* polymerase; the cycling protocol was: 3 min at 95°C, 2 cycles: 30 s at 94°C, 1 min at 58°C, 5 min at 72°C, then cDNA library was removed and amplification proceeded with another 37 cycles: 30 s at 94°C, 1 min at 58°C, 1 min at 72°C, 7 min at 72°C.

Quantitative real-time PCR

The hybridization primer/probe assays for real-time PCR detection were purchased from Applied Biosystems. The following assay-on-demand probes were used: GAPDH: P/N 4308313, β_2-microglobulin: Rn00560865_m1, TASK1: Rn00583727_m1, HCN1: Rn00584498_m1, HCN3: Rn00586666_m1, HCN4: Rn00572232_m1. The designed probes were: TASK3, forward: TCC TTC TAC TTC GCT ATC ACT GTC A, reverse: TTG CCA GCA TCG GTT CCA, reporter: CAT GTC CAT ATC CGA TAG TTG; HCN2, forward: ACA AGG AGA TGA AGC TGT CAG ATG, reverse: TGT CAG CCC GCA CAC T, reporter: CAG ATC TCC CCA AAA TAG. Real-time PCR was performed using the ABI Prism 7000 Sequence Detection System (Applied Biosystems, Darmstadt, Germany); PCR program was: 2 min at 50°C, 10 min at 95°C, 40 cycles: 15 s at 95°C and 1 min at 60°C. Results were analyzed with the ABI Prism 7000 SDS software. The efficiency of real-time primers was assessed by plotting Ct values versus corresponding dilution factor of total thalamic cDNA. Linear regression revealed slope factors that were maximally 8% different between β_2-microglobulin, TASK1, TASK3, and HCN2.

RESULTS

Expression of HCN and TASK channel isoforms in rat dLGN

In a first experimental step, the expression of different HCN and TASK channel isoforms was determined through RT-PCR analysis on dLGN tissue. Strong signals for TASK1 and TASK3 were found, whereas TASK2 was less expressed and TASK5 was not detectable (Fig. 1*A*, *left*). To determine the expression of TASK isoforms on a more quantitative level, we subjected TASK1 and TASK3 mRNAs to a real-time PCR approach. Expression levels of TASK3 were 4.4 ± 0.2-fold ($n = 3$) higher compared with TASK1 (Fig. 1*D*, *left*) after normalization to the constitutively expressed housekeeping gene β_2-microglobulin. Similar expression ratios were found for cortical (3.6 ± 0.1; $n = 3$) and hippocampal (3.5 ± 0.1; $n = 3$) tissues that were used for comparison (data not shown). When cerebellar tissue, known to express high levels of TASK1, was tested, the TASK3/TASK1 expression ratio was 0.7 ± 0.1 ($n = 3$). Expression of HCN channels was assessed in a similar way. Standard PCR protocols revealed the expression of all four HCN isoforms (Fig. 1*A*, *right*). Real-time PCR was used to attain more quantitative results of isoform expression. The expression level of HCN2 could be assessed to be

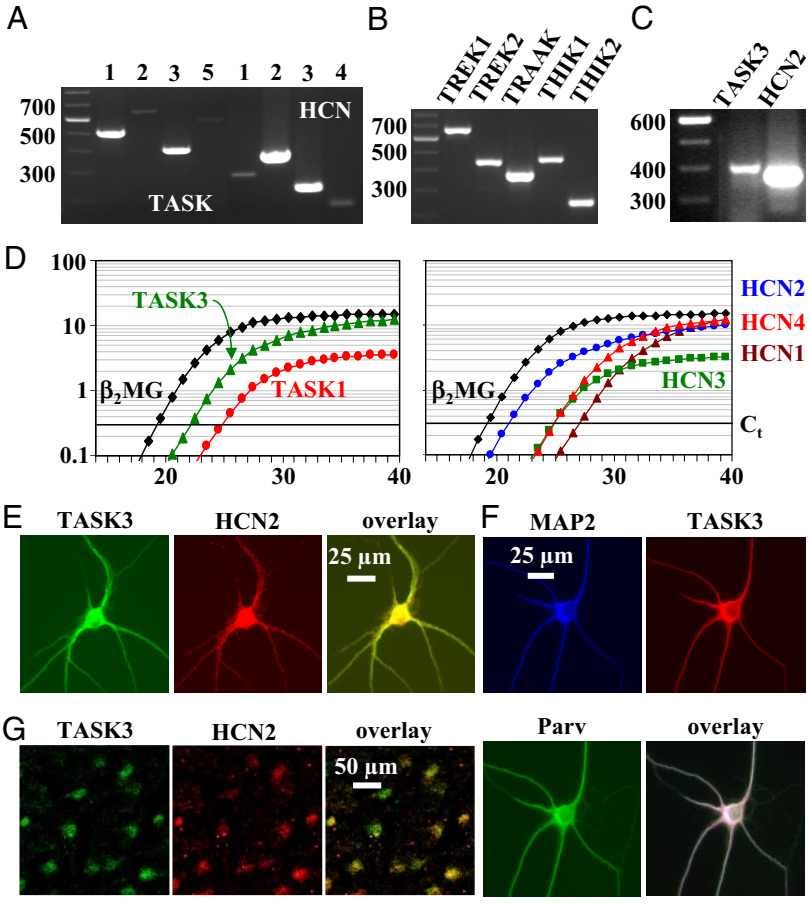

FIG. 1. Reverse transcription–polymerase chain reaction (RT-PCR) and immunological analysis of rat thalamic tissue. *A*: expression of TASK1–5 and HCN1–4 channels in dorsal lateral geniculate nucleus (dLGN) revealed by standard RT-PCR. *B*: expression of K_{2P} channels in dLGN revealed by standard RT-PCR. *C*: coexpression of HCN2 and TASK3 in identified thalamocortical relay (TC) neurons revealed by standard RT-PCR. *D*: quantitative real-time RT-PCR analysis of TASK1 and TASK3 and HCN1–4 expression in comparison to β_2-microglobulin (β_2-MG) in dLGN tissue. Number of cycles is plotted vs. normalized and baseline corrected fluorescence (ΔRn). *E* and *F*: immunohistochemical localization of TASK3 (green fluorescence) and HCN2 (red fluorescence) in cell culture (*E*) and brain slices (*F*). Overlay (*right*) reveals coexpression of both ion channel proteins. *G*: immunohistochemical localization of microtubule associated protein 2 (MAP2; blue fluorescence), a neuron-specific marker, parvalbumin (green fluorescence), a TC neuron–specific marker, and TASK3 (red fluorescence) in thalamic neurons in cell culture. Overlay (*right*) reveals the coexpression of all 3 proteins.

7.5 ± 0.1-fold higher compared with HCN3 and HCN4, and 12 ± 0.1-fold ($n = 3$) higher compared with HCN1 (Fig. 1*D*, *right*). Together with earlier results obtained from HCN2-deficient mice (Ludwig et al. 2003), TASK1-deficient mice (Meuth et al. 2006), and Long–Evans rats (Meuth et al. 2003) we concluded that HCN2 and TASK3 are the dominant isoforms in dLGN.

The expression of other members of the K_{2P} family of ion channels (Patel and Lazdunski 2004) was probed by RT-PCR on the tissue level. The use of specific primer pairs revealed the presence of TREK-1, TREK-2, TRAAK, THIK-1, and THIK-2 mRNA in dLGN tissue (Fig. 1*B*).

Next, the cellular localization of HCN2 and TASK3 channels was determined. Neurons were acutely isolated from the dLGN, TC neurons were identified in populations of neurons using established criteria (Pape et al. 1994), and groups of 10 TC neurons were harvested for RT-PCR analysis. The use of HCN2- and TASK3-specific primer pairs revealed detectable PCR signals for the two ion channels (Fig. 1*C*). Furthermore, TASK3- and HCN2-specific antibodies revealed a dense population of HCN2 (716 ± 17 cells/mm^2; Fig, 1*G*, *middle image*) and TASK3 607 ± 29 cells/mm^2; Fig. 1*G*, *left image*) expressing cells in dLGN slices (five independent preparations). Furthermore the overlap of images revealed 604 ± 26 cells/mm^2 (Fig, 1*G*, *right image*) with co-localization of both channels. The average cell density in Nissl staining was 808 ± 31 cells/mm^2 ($n = 6$; coronal sections of 14 μm thickness), indicating that 89, 75, and 75% of the cells express HCN2, TASK3, and HCN2/TASK3, respectively, thereby providing evidence for largely overlapping expression. In thalamic cell cultures (DIV 21), 100% of TC neurons (a total of 30 TC neurons were identified in 10 different cultures from three independent preparations) were positive for TASK3 (Fig. 1*E*, *left image*) and HCN2 (Fig. 1*E*, *middle image*). Their localization in TC neurons (a total of 24 cells were identified in eight different cultures from three independent preparations) was further demonstrated by the finding that parvalbumin (Fig. 1*F*, *bottom left image*), a specific marker protein of TC neurons (Jones and Hendry 1989; Meuth et al. 2005; Sieg et al. 1998), was expressed in TASK3- (Fig. 1*F*, *top right image*) and MAP2-positive neurons (Fig. 1*E*, *top left image*).

Characterization of pH-sensitive ramp currents

In the following extracellular pH changes from a physiological value of 7.3 (control) to 6.3, a value that is reached during ischemic insults (Siemkowicz and Hansen 1981) were used to demonstrate the functional interaction of HCN and TASK channels in TC neurons. Because currents through HCN and TASK channels are sensitive to extracellular acidification (Malcolm et al. 2003; Meuth et al. 2003; Stevens et al. 2001), this experimental paradigm results in a concomitant downregulation of both $I_{K\text{-leak}}$ and I_h. Currents through TASK channels were evoked by holding TC neurons at −30 mV and ramping the potential in 800 ms to −120 mV once every 20 s (Fig. 2*A*, *inset*). The rate of hyperpolarization 0.11 mV/ms is sufficiently slow to allow the membrane current to reach steady state at each potential and it is expected that only constitutively open channels can follow the ramp (Millar et al. 2000; Watkins and Mathie 1996). The current–voltage (*I–V*) relationship of the pH-sensitive current was obtained by subtracting currents recorded at pH 6.3 from control currents (i.e., pH 7.3 − pH 6.3). The *I–V* relationship of the pH-sensitive currents (about 10 min after extracellular acidification) was characterized by outward rectification (Fig. 2*A*, *gray trace*) and a reversal potential of −90 ± 2 mV ($n = 10$; Fig. 2*B*, gray circle), i.e., some 14 mV positive to the expected K^+ equilibrium potential ($E_K = -104$ mV). To demonstrate that pH-dependent regulation of I_h contributed to the deviation the HCN channel blocker ZD7288 was used. Incubation of TC neurons with 100 μM ZD7288 before

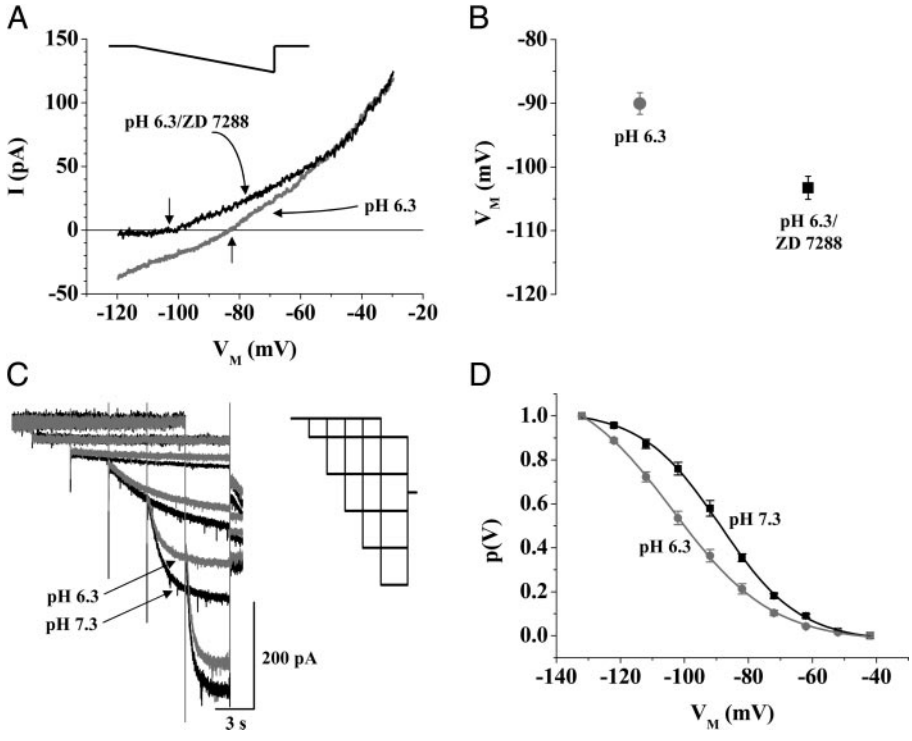

FIG. 2. Current components sensitive to extracellular acidification in TC neurons. *A*: current-to-voltage relationship (*I–V*) of the pH-sensitive current obtained by graphical subtraction (pH 7.3 − pH 6.3) in the presence (*black trace*) and absence (*gray trace*) of ZD7288 (100 μM). Currents were evoked by ramping the membrane from −30 to −120 mV over 800 ms (see *inset*). *B*: mean values of the reversal potential of pH-sensitive ramp current in the presence (black square) and absence (gray circle) of ZD7288. *C*: superimposed families of *current traces* recorded at pH 7.3 (*black traces*) and 6.3 (*gray traces*) in a rat TC neuron. *Current traces* at −53, −73, −93, −113, and −133 mV are shown. *Inset*: clarifies the voltage protocol. *D*: mean steady-state activation curves of I_h at pH 7.3 (black squares; $n = 7$) and pH 6.3 (gray circles; $n = 7$). Continuous lines represent best fits of a Boltzmann equation to the data points.

extracellular acidification was performed resulted in an *I–V* relationship of pH-sensitive ramps that revealed the typical features of a current carried by TASK channels (Meuth et al. 2003), including pronounced outward rectification (Fig. 2*A*, *black trace*) and a significantly ($P < 0.0001$) more hyperpolarized reversal potential of -103 ± 2 mV ($n = 8$; Fig. 2*B*, black square), i.e., close to the expected K^+ equilibrium potential.

To directly prove the modulation of HCN channels by extracellular acidification, we activated I_h from a holding potential of -43 mV by using hyperpolarizing voltage steps of increasing ($\Delta V = -10$ mV) amplitude and decreasing ($\Delta t = -1{,}500$ ms) duration (15.5 s at -53 mV to 3.5 s at -133 mV) followed by a constant step to -98 mV (Fig. 2*C*, *inset*). Recordings were performed in the presence of 150 μM Ba^{2+} to block TASK and inward rectifier channels (Meuth et al. 2003). An analysis of deactivating currents revealed a half-maximal value of I_h activation at a membrane potential of -87 ± 2 mV ($n = 7$) at pH 7.3 (Fig. 2*D*, black squares). Ten minutes after switching the extracellular solution from pH 7.3 to pH 6.3, half-maximal activation of I_h was significantly ($P = 0.00001$) shifted to -100 ± 1 mV ($n = 7$; Fig. 2*D*, gray circles). To ensure that this effect was not a result of run-down phenomena, I_h protocols were delivered in 10-min intervals under control conditions in a different set of experiments. No significant ($P = 0.153$) differences could be found under these recording conditions (first protocol: -86 ± 3 mV; second protocol: -84 ± 3 mV; $n = 4$; data not shown). In conclusion these findings indicated a contribution of both HCN and TASK channels to the pH-sensitive current component in dLGN TC neurons and point to an opposing functional influence on membrane excitability.

Effect of extracellular acidification on thalamic activity modes

The functional consequence of concomitant modulation of HCN and TASK channels by acidification was probed under current-clamp conditions. To ensure robust burst responses, recordings were obtained at slightly hyperpolarized values ($V_H = -73 \pm 1$ mV, $n = 12$; Fig. 3*A*) of the membrane potential with respect to the resting value (V_R) of -71 ± 1 mV ($n = 25$; Fig. 3*A*) using DC injection. Under these conditions, depolarizing current steps elicited high-frequency ($f_H = 134 \pm 10$ Hz, $n = 6$; Fig. 3*B*) bursts with two to five action potentials riding on top of a low-threshold Ca^{2+} spike (Fig. 3*C*). Changing the extracellular pH from 7.3 to 6.3 resulted in a nonsignificant depolarization of the membrane potential to $V_{pH6.3} = -68 \pm 1$ mV (Fig. 3*A*), during which burst firing ($f_{pH6.3} = 113 \pm 1$ Hz; Fig. 3*B*) was preserved (Fig. 3*D*; $n = 5$). Different results were obtained in the presence of ZD7288. Application of ZD7288 resulted in a significant ($P < 0.01$) hyperpolarization of the resting membrane potential (V_{ZD}) to -79 ± 2 mV ($n = 7$; Fig. 3*A*). After bringing the membrane potential back to the control level of about -72 mV using DC current injection, a step depolarization revealed that burst firing ($f_{ZD/H} = 136 \pm 11$ Hz; $n = 6$; Fig. 3*B*) persisted (Fig. 3*E*). Subsequent extracellular acidification resulted in a strong depolarization of the membrane potential ($V_{ZD/pH6.3}$) to -52 ± 3 mV ($n = 6$; Fig. 3*A*) accompanied by a change in firing mode from burst to tonic ($f_{ZD/pH6.3} = 32 \pm$ Hz, $n = 6$; Fig. 3, *B* and *F*). These findings show that extracellular acidification results in a net depolarization of TC neurons. The magnitude and, in consequence, the functional relevance of this depolarization is controlled by an interplay between TASK and HCN channels. The

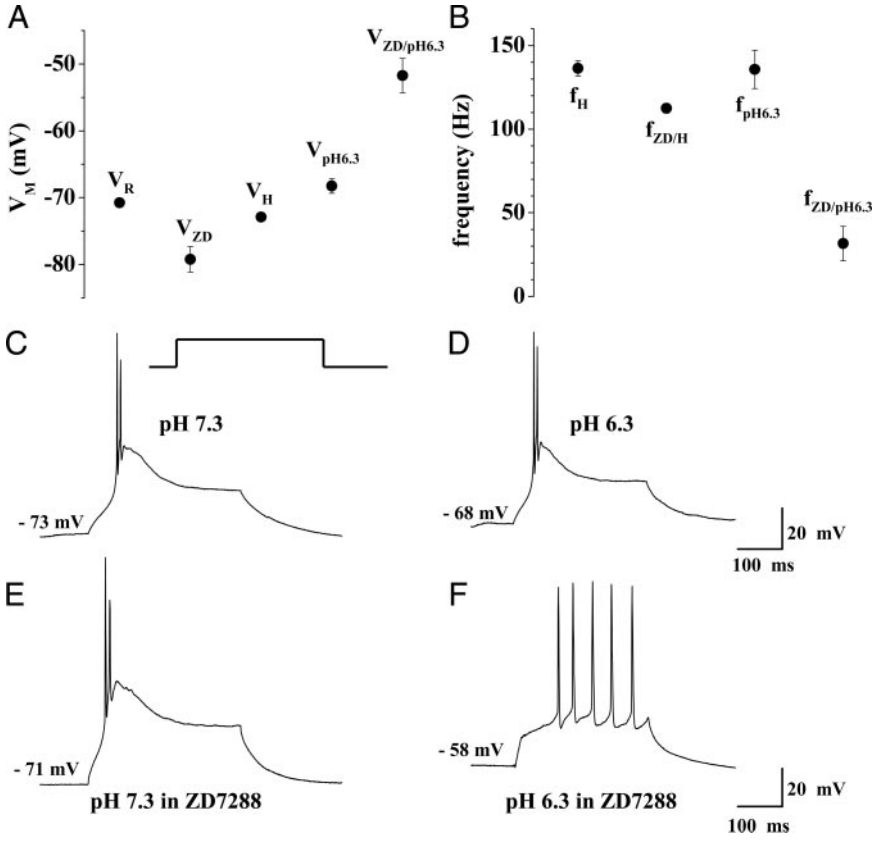

FIG. 3. Effect of extracellular acidification on thalamic activity modes in rat TC neurons recorded under current-clamp conditions. *A*: mean values of resting membrane potentials under different recording conditions. V_R, resting potential under control conditions; V_{ZD}, resting potential in the presence of 100 μM ZD7288; V_H, holding level of the membrane potential achieved by DC current injection; $V_{pH6.3}$, resting potential at pH 6.3; $V_{ZD/pH6.3}$, resting potential at pH 6.3 in the presence of ZD7288. *B*: mean firing frequencies under different recording conditions. Firing frequency was determined for the first 2 action potentials elicited by the depolarizing pulse. f_H, firing frequency at V_H; $f_{ZD/H}$, firing frequency at V_H in the presence of ZD7288; $f_{pH6.3}$, firing frequency at pH 6.3; $f_{ZD/pH6.3}$, firing frequency at pH 6.3 in the presence of ZD7288. *C–F*: depolarizing current pulses (300-ms duration, 100–200 pA) from a control potential (V_H) of about -73 mV elicited robust burst responses in the absence (*C*) and presence (*E*) of ZD7288. Extracellular acidification results in a depolarizing shift of the membrane potential and generation of tonic trains of action potentials in response to the same depolarizing current pulse in the presence (*F*), but not in the absence (*D*), of ZD7288.

main characteristics of the two thalamic activity modes with high-frequency burst firing at hyperpolarized potentials and low-frequency tonic firing at depolarized potentials were unchanged.

Next the role of the HCN2 isoform was assessed through the use of a mouse strain deficient of HCN2 channels ($HCN2^{-/-}$) (Ludwig et al. 2003). The resting membrane potentials of TC neurons in wild-type ($HCN2^{+/+}$) mice ($V_{R/HCN2+/+} = -69 \pm 1$ mV, $n = 22$; Fig. 4*A*) were significantly ($P < 0.01$) more positive compared with $HCN2^{-/-}$ mice ($V_{R/HCN2-/-} = -81 \pm 1$ mV, $n = 21$; Fig. 4*A*), confirming previous findings (Ludwig et al. 2003). A change of extracellular pH from 7.3 to 6.3 in cells held at a potential (V_H) of -73 ± 1 mV using DC current injection ($n = 8$; Fig. 4, *A* and *C*) resulted in a nonsignificant hyperpolarization of the membrane potential ($V_{pH6.3/HCN2+/+}$) to -75 ± 1 mV in $HCN2^{+/+}$ mice ($n = 6$; Fig. 4, *A* and *D*). At pH 7.3 and pH 6.3 cells fired high-frequency bursts of action potentials with intraburst frequencies of $f_{HCN2+/+} = 114 \pm 2$ Hz and $f_{pH6.3/HCN2+/+} = 111 \pm 6$ Hz, respectively ($n = 6$; Fig. 4*B*). In $HCN2^{-/-}$ mice held at -73 mV under control conditions the intraburst frequency was $f_{HCN2-/-} = 111 \pm 2$ Hz ($n = 5$; Fig. 4, *B* and *E*). At pH 6.3 TC neurons were significantly ($P < 0.01$) more depolarized with $V_{pH6.3/HCN-/-} = -58 \pm 2$ mV ($n = 5$; Fig. 4, *A* and *F*) and revealed tonic firing ($f_{pH6.3/HCN2-/-} = 33 \pm 7$ Hz, $n = 5$; Fig. 4, *B* and *F*). These data indicate that HCN2 channels carry a major part of I_h function in TC neurons.

Steady-state current components in TC neurons

Ion channels suitable to determine V_R should be able to sustain a steady-state current. To determine the contribution of different current components, cells were kept at a holding potential of -68 mV. Under these recording conditions TC neurons displayed a standing outward current (I_{SO}) with an amplitude of 71 ± 4 pA ($n = 10$). In a first experimental step, a pharmacological profile of this current was obtained by cumulative application of different ion channel modulators. Figure 5 shows the time course of a typical experiment (Fig. 5*A*, open squares). Washin of tetrodotoxin (TTX, 1 μM) had no effect, application of the I_h channel blocker ZD7288 (100 μM) significantly increased, and lowering the extracellular pH from 7.3 to 6.3 significantly decreased I_{SO}. Addition of Ba^{2+} (150 μM) and tetraethylammonium (TEA, 20 mM)/4-aminopyridine (4-AP, 6 mM) resulted in a further significant reduction of the outward current.

To increase outward current amplitudes, recordings were obtained at more depolarized values of the membrane potential. At -28 mV (Fig. 5*A*, closed squares), I_{SO} averaged 343 ± 15 pA ($n = 51$). TTX (1 μM) resulted in an increase in current amplitude of $7 \pm 1\%$ ($n = 9$) and additional application of ZD7288 (100 μM) decreased the current ($6 \pm 2\%$, $n = 9$). Changing the external pH from 7.3 to 6.3 in the continuous presence of TTX and ZD7288 induced a further decrease by $42 \pm 3\%$ ($n = 5$). Addition of Ba^{2+} (150 μM) and TEA (20 mM)/4-AP (6 mM) led to a further decrease by 49 ± 6 and $82 \pm 5\%$ ($n = 5$), respectively. All drug effects were statistically significant with respect to current amplitudes under control conditions. In the presence of all blocking agents, the current was almost completely blocked (9 ± 5 pA residual current; $n = 5$). These results are consistent with the hypothesis that Na^+ channels, I_h channels, pH-sensitive TASK channels, Ba^{2+}-sensitive Kir and leak channels, and TEA/4AP-sensitive voltage-dependent K^+ channels

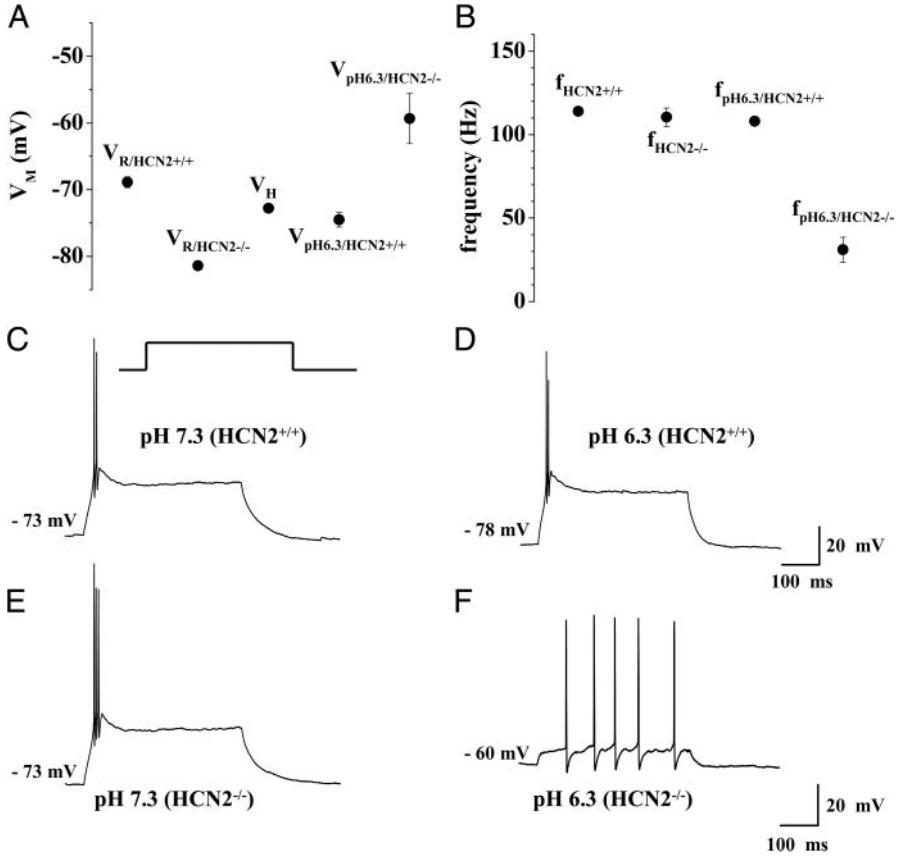

FIG. 4. Effect of extracellular acidification on thalamic activity modes in mice. *A*: mean values of resting membrane potentials under different recording conditions. $V_{R/HCN2+/+}$, resting potential under control conditions in $HCN2^{+/+}$ mice; $V_{R/HCN2-/-}$, resting potential under control conditions in $HCN2^{-/-}$ mice; V_H, holding level of the membrane potential achieved by DC current injection; $V_{pH6.3/HCN2+/+}$, resting potential at pH 6.3 in $HCN2^{+/+}$ mice; $V_{pH6.3/HCN2-/-}$, resting potential at pH 6.3 in $HCN2^{-/-}$ mice. *B*: mean firing frequencies under different recording conditions. Firing frequency was determined for the first 2 action potentials elicited by the depolarizing pulse. $f_{HCN2+/+}$, firing frequency at V_H in $HCN2^{+/+}$ mice; $f_{HCN2-/-}$, firing frequency at V_H in $HCN2^{-/-}$ mice; $f_{pH6.3/HCN2+/+}$, firing frequency at pH 6.3 in $HCN2^{+/+}$ mice; $f_{pH6.3/HCN-/-}$, firing frequency at pH 6.3 in $HCN2^{-/-}$ mice. *C* and *D*: depolarizing current pulses (400-ms duration, 100–200 pA) were applied from a holding potential of about -73 mV. In TC neurons from $HCN2^{+/+}$ mice pulse depolarization elicited a burst response at pH 7.3 (*C*) and pH 6.3 (*D*). *E* and *F*: in TC neurons from $HCN2^{-/-}$ mice pulse depolarization elicited a burst response at pH 7.3 (*E*). Extracellular acidification resulted in a depolarizing shift of the membrane potential and generation of tonic trains of action potentials in response to the same depolarizing current pulse (*F*).

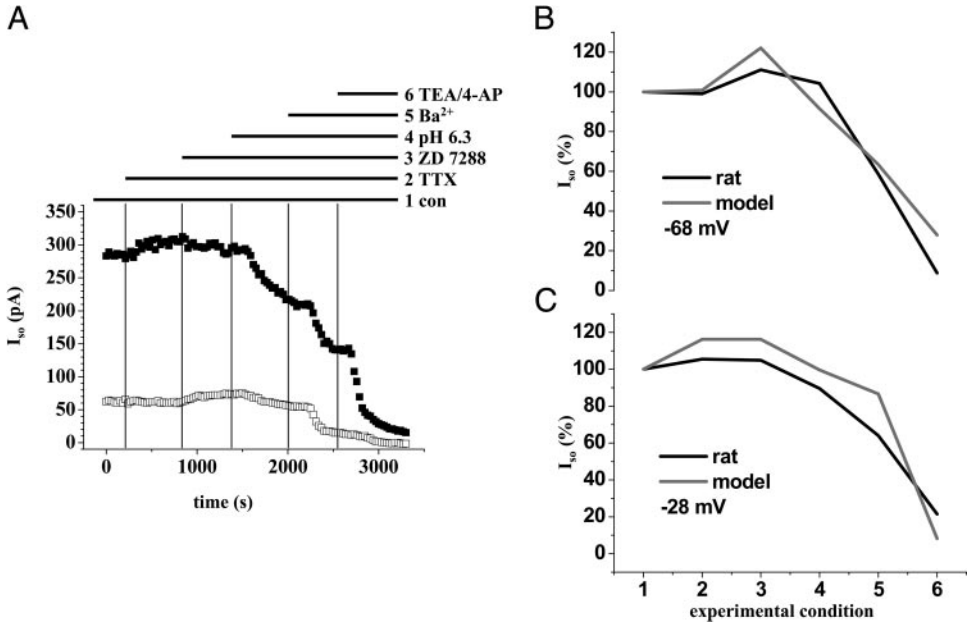

FIG. 5. Pharmacological profile of the standing outward current in thalamocortical relay neurons at different holding potentials. *A*: amplitude of the net outward current plotted against time in a relay neuron recorded under voltage-clamp conditions at −28 mV (black data points) and −68 mV (open data points) under the following experimental conditions (1–6): 1, control conditions; 2, during cumulative application of TTX (1 μM); 3, ZD7288 (100 μM); 4, H^+ (pH 7.3–6.3); 5, Ba^{2+} (150 μM); 6, TEA/4-AP (20 mM/6 mM), as indicated by horizontal lines. Holding current was recorded every 20 s for a duration of 800 ms. *B* and *C*: comparison of averaged data from recordings in 5 neurons (*black traces*) and computer modeling (*gray traces*) at −68 mV (*B*) and −28 mV (*C*). Normalized I_{SO} amplitudes are plotted vs. time. Recording conditions as in *A*. For reduction of currents in the model cell see text.

constitute I_{SO} in TC neurons with the degree of their contribution depending on the value of the holding potential.

Computer modeling of steady-state current in TC neurons

We modified an existing TC neuron model (Huguenard and McCormick 1992; McCormick and Huguenard 1992) by adding an inward rectifier K^+ current (Williams et al. 1997) and substituting the linear characteristic of $I_{K\text{-leak}}$ by a Goldman–Hodgkin–Katz (GHK) formalism (Meuth et al. 2005). Furthermore we made 49% of $I_{K\text{-leak}}$ (default value = 10 nS) sensitive to changes in pH and designated this component as the outwardly rectifying TASK current (I_{TASK}). This assumption was based on previous and above findings indicating that the current through TASK channels makes up about 38–59% of I_{SO} in rodent TC neurons (Meuth et al. 2003, 2006; Musset et al. 2006).

Next, the consecutive pharmacological manipulation of I_{SO} was analyzed using the model cell. Current changes at a holding potentials of −68 mV (Fig. 5*B*) and −28 mV (Fig. 5*C*) were compared with averaged experimental data (black lines, $n = 5$). Although a 90% reduction of I_{NaP} (TTX effect) resulted in a 16% increase in I_{SO} at −28 mV with no effect at −68 mV, 90% block of I_h (ZD7288 effect) had no effect at −28 mV but increased I_{SO} by 22% at −68 mV. Reduction (the remaining current is stated in %) of I_{TASK}, I_{Kir}, $I_{K\text{-leak}}$, and the delayed rectifier K^+ current (I_{DR}) was used to simulate extracellular acidification (I_{TASK}: 25%), block by Ba^{2+} (I_{TASK}: 0%; I_{Kir}: 10%; $I_{K\text{-leak}}$: 90%), and block by TEA/4-AP (I_{Kir}: 0%; $I_{K\text{-leak}}$: 70%; I_{DR}: 55%). In addition the transient K^+ outward current (I_A) was assumed to be completely 4-AP sensitive. As shown in Fig. 5, *B* and *C*, the model cell (gray lines) reliably describes the qualitative changes of I_{SO} in rats (black lines) with a mean deviation between modeled and measured current amplitudes of 12 ± 2% ($n = 10$; averaged over all experimental conditions at two holding potentials).

Next we used computer modeling techniques to assess the relative contribution of HCN and TASK channels to the pH effects. The resting membrane potential of the model cell was $V_1 = -72$ mV (Fig. 6*A*). From this potential a step depolarization evoked a low-threshold Ca^{2+} spike and a high-frequency burst ($f_1 = 102$ Hz; Fig. 6*B*) of action potentials (Fig. 6*C*). The effect of extracellular acidification was simulated by simultaneously reducing the maximal conductance of I_h and I_{TASK} by 25% (Munsch and Pape 1999) and 90% (Meuth et al. 2003) of their initial values, respectively. As a result the membrane potential of the model cell depolarized to $V_2 = -68$ mV (Fig. 6*A*) with burst firing ($f_2 = 112$ Hz; Fig. 6*B*) being preserved (Fig. 6*D*). Next, the block of HCN channels by ZD7288 was simulated by removing I_h from the computer model, resulting in membrane hyperpolarization to $V_3 = -82$ mV (Fig. 6*A*). Using DC-current injection the membrane potential of the model cell was reset to $V_{3/DC} = -72$ mV (Fig. 6*A*) and a subsequent step depolarization elicited a burst response ($f_{3/DC} = 105$ Hz; Fig. 6, *B* and *E*). Next, extracellular acidification was simulated by removing 90% of I_{TASK}, thereby leading to a depolarization of the membrane potential to −58 mV (Fig. 6*A*) accompanied by tonic firing ($f_{4/DC} = 19$ Hz; Fig. 6, *B* and *F*). In an additional set of simulations the upregulation of I_h (e.g., by cAMP) was modeled by increasing the default value of I_h conductance by 25% (data not shown). As a consequence the resting membrane potential of the model cell was depolarized to $V_1 = -70$ mV. Simulation of extracellular acidification depolarized the membrane potential to $V_2 = -66$ mV, thereby shifting the model to an intermediate firing mode (LTS crowned by a single action potential and followed by tonic firing of three action potentials).

Taken together these findings indicate an opposing interaction of TASK3/TASK1 and HCN2 channels to stabilize the resting membrane potential of TC neurons.

Because a number of components contribute to I_{SO} we expanded our modeling approach. Different combinations of hyperpolarizing (I_{Kir}, $I_{K\text{-leak}}$, I_{TASK}) and depolarizing (I_h, I_{NaP}) currents were modulated and compared with the effect seen in rats (Fig. 7). The following experimental conditions were analyzed: *1*) Control conditions represent V_R of the model cell (−72 mV) and mean V_R of rat TC neurons (−71 ± 1 mV, $n =$

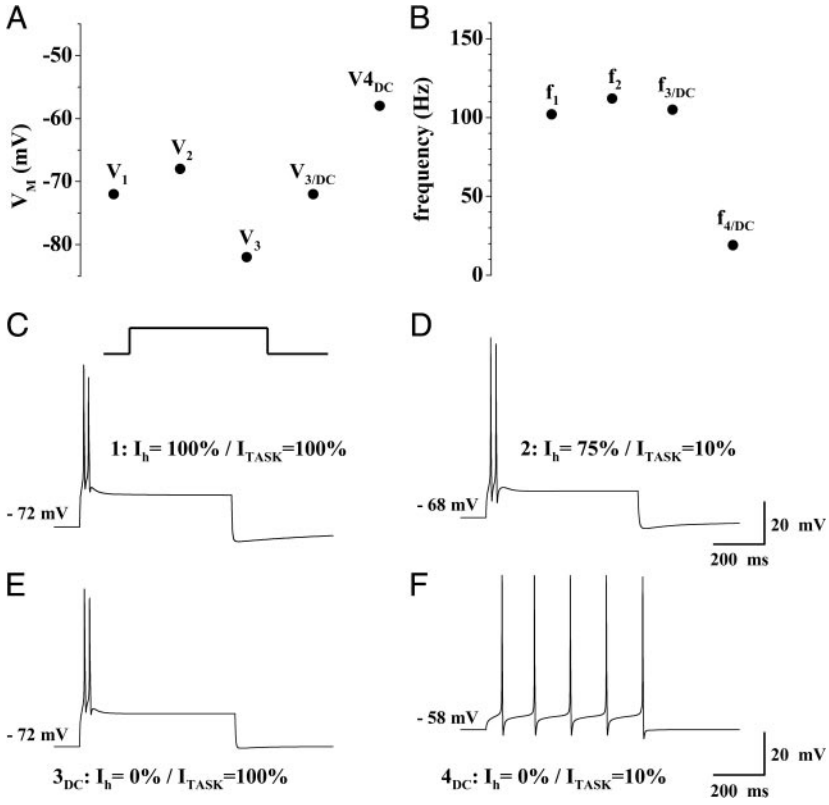

FIG. 6. Computer simulation of activity modes in rat TC neurons. *A* and *B*: resting membrane potentials and firing frequencies of the model cell under different conditions: Control conditions (V_1, f_1); with I_h (the current through HCN channels) and I_{TASK} (the current through TASK channels) reduced by 25 and 90%, respectively, (V_2, f_2); without I_h (V_3); without I_h and the membrane potential reset to the control level ($V_{3/DC}$, $f_{3/DC}$); without I_h, DC current injection, and 90% reduction of I_{TASK} ($V_{4/DC}$, $f_{4/DC}$). *C*: depolarizing current pulses (300-ms duration, 150 pA) were applied from a potential of −72 mV. With I_h and I_{TASK} set to 100%, the membrane resting potential settled at −72 mV. A step depolarization resulted in a burst response. *D*: setting I_h and I_{TASK} to 75 and 10%, respectively, resulted in a membrane depolarization to −68 mV and a burst of action potentials after a depolarizing current step. *E*: with I_h and I_{TASK} set to 0 and 100%, respectively, a DC current injection of 150 pA was necessary to set the resting potential to a value of −72 mV. A step depolarization resulted in a burst of action potentials. *F*: setting I_h and I_{TASK} to 0 and 10%, respectively, resulted in a membrane depolarization to −58 mV and a tonic train of action potentials following a depolarizing current step.

25) recorded in slices. *2*) During extracellular acidification (pH 6.3) both 25 and 90% reductions of I_h and I_{TASK} were assumed in native cells, respectively. Therefore in the model cell the indicated depolarizing and hyperpolarizing current was reduced by 25 and 90%, respectively. The resulting changes in V_R are shown. *3*) The block of I_h hyperpolarizes native TC neurons and the model cell. To reach the control level of V_M (about −73 mV) positive DC currents of 100–200 and 150 pA were injected to native TC neurons and the model cell, respectively. Furthermore, the indicated depolarizing current was removed in the model cell. *4*) The last experimental condition simulates the effect of reducing the indicated hyperpolarizing current by 90%, whereas the indicated depolarizing current was removed from the computer model and a positive current of +150 pA was injected. As shown in Fig. 7, only the combined modulation of I_{TASK}/I_h and $I_{K\text{-}leak}/I_h$ closely matched the experimental data from rats. It is interesting to note that the use of a linear $I_{K\text{-}leak}$ component was less effective in reproducing whole cell patch-clamp recordings (data not shown).

Taken together, these data show that the joined modulation of I_{TASK} and I_h is the most likely cellular action that account for the pH effect seen in native TC neurons.

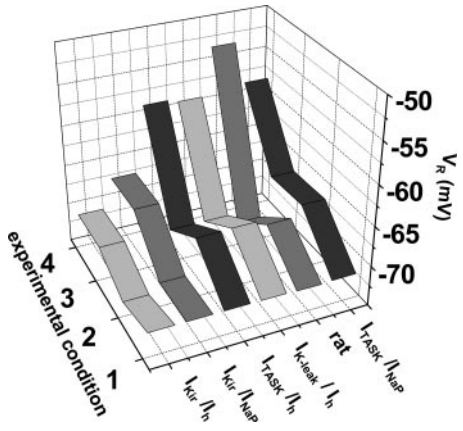

FIG. 7. Modeling the effect of hyperpolarizing (I_{Kir}, $I_{K\text{-}leak}$, I_{TASK}) and depolarizing (I_h, I_{NaP}) membrane currents on V_{rest}. Different pairs of currents (as indicated) were altered in a computer model to reproduce the results found in native rat TC neurons. Experimental conditions were as follows: 1, control condition: V_{rest} of the model cell and mean V_R of rat TC neurons. 2, pH 6.4: in native TC neurons a 25 and 90% reduction of I_h and I_{TASK} was assumed, respectively. Therefore in the model cell the indicated depolarizing and hyperpolarizing current was reduced by 25 and 90%, respectively. 3, block of I_h and injection of +150-pA DC current in native TC neurons. In the model cell the indicated depolarizing current was eliminated and +150-pA DC current was injected. 4, pH 6.4 and block of I_h during DC current injection. In the model cell the indicated depolarizing current was eliminated, the indicated hyperpolarizing current was reduced by 90% and +150-pA DC current was injected. Note that only the combination I_{TASK}/I_h and $I_{K\text{-}leak}/I_h$ closely matches the native situation (rat).

DISCUSSION

The main results of the present paper can be summarized as follows. *1*) All known pacemaker channels (HCN1–4), TASK1–3 channels, and at least five other members of the K_{2P} channel family (TREK1, TREK2, TRAAK, THIK1, THIK2) are expressed in rat dLGN. *2*) The dominant isoforms, HCN2 and TASK3, are coexpressed in TC neurons. *3*) Current components carried by HCN and TASK channels contribute to the pH-sensitive component elicited by hyperpolarizing ramp protocols in TC neurons. *4*) Extracellular acidification leads to depolarization of TC neurons the magnitude of which critically depends on the availability of HCN and TASK channels. Current-clamp recordings in rats, $HCN2^{-/-}$ mice, and computer modeling studies demonstrate that the counterbalancing

effects of HCN2 and TASK3/TASK1 channels play an important role in setting the resting membrane potential of TC neurons. *5*) Although modulation of TASK and/or HCN channels can effectively shift TC neurons between firing modes, the overall characteristics of the two forms of activity are rather unchanged.

pH-sensitive membrane currents in TC neurons

TASK1 and TASK3 channels, which are sensitive to changes in extracellular pH (Duprat et al. 1997; Kim et al. 2000; Rajan et al. 2000), are expressed in TC neurons (Meuth et al. 2003). Thus pH-sensitive currents evoked by hyperpolarizing voltage ramps revealed typical features of a current carried by TASK channels. However, the reversal potential deviated from that of a pure K^+ current. Even more surprising, in contrast to the inhibition of TASK channels by bupivacaine and muscarine (Meuth et al. 2003), the closure of TASK channels by external H^+ ions did not result in a strong depolarization of the membrane potential. Only after blocking I_h, pH-sensitive ramp currents reversed at the expected K^+ reversal potential and extracellular acidification induced a strong depolarization, thereby proving the contribution of both HCN and TASK channels to the pH-sensitive component.

The counterbalancing modulation of TASK and HCN channels restricts the net effect of acidification on the resting membrane potential. The experimental paradigm used to demonstrate this interaction included the use of DC current injection to achieve similar control values of the membrane potential (about −72 mV). This was done to exemplify the different effects of acidification with (no shift in activity mode) and without I_h (shift in activity mode), rather than to mimic a sequence of events in the brain. The scenario of interacting TASK and HCN channels is strengthened by the fact that V_R values of TASK1-deficient mice are significantly more depolarized compared with wild-type animals under control conditions and in the presence of ZD7288 (Meuth et al. 2006).

Based on results obtained from rat (Meuth et al. 2003; Musset et al. 2006), TASK1-KO mice (Meuth et al. 2006), and computer modeling (this study) it can be concluded that the pH-sensitive component (acidification to pH 6.3) makes up about 40% of I_{SO} (at −28 mV). However, at extracellular pH values exceeding the modulation range of TASK channels (i.e., pH <6.0) I_{SO} is further reduced, indicating the presence of additional pH-sensitive components. To assess whether other ion currents may mediate the pH effect seen in the present study, we used computer modeling. Not one combination, including I_{Kir} or I_{NaP}, was able to account for the result obtained from TC neurons. Nevertheless the contribution of more components cannot be fully excluded because changes in extracellular pH can modulate the activity of a variety of ion channels and receptors (for review see Kaila and Ransom 1998). Furthermore, subtle differences between cellular properties may account for differences in the pH effect under control conditions seen in rat (depolarization) and mice (hyperpolarization). This view is corroborated, for example, by the finding that TASK3 is clearly the dominant subtype in rat but TASK1 and TASK3 reveal roughly equal mRNA levels in mouse dLGN (Meuth et al. 2006). Similar considerations may apply to HCN channels that show functional expression of HCN1 in rat (Budde et al. 2005) but not in mouse TC neurons (Franz et al. 2000).

Constituents of the resting membrane potential in TC neurons

The resting membrane potentials of TC neurons in different species and thalamic nuclei are reportedly in the range of −60 to −75 mV (McCormick and Pape 1990; Meuth et al. 2003; Porcello et al. 2003; Williams et al. 1997; Zhan et al. 1999), the evolution of which is ascribed to leak currents ($I_{K\text{-leak}}$, $I_{Na\text{-leak}}$), pacemaker currents (I_h), inwardly rectifying K^+ currents (I_{KIR}), voltage-dependent currents active below threshold (I_A, I_T), and any DC current experimentally injected to the cell (I_{inj}) (Williams et al. 1997; Zhan et al. 1999). In agreement with this assumption the standing outward current of TC neurons (Meuth et al. 2003) is composed of I_h, I_{Kir}, I_{TASK}, a persistent Na^+ current, and voltage-denpendent K^+ currents. The results of the present study allow the assignment of most of the I_h component to HCN2 channels.

The evidence to support the hypothesis that I_h is active at the resting membrane potential of TC neurons under the present recording conditions (−71 mV) is as follows. I_h is a slow inward current activating at potentials negative to −55 mV (see Fig. 2*D*), shows no inactivation (McCormick and Pape 1990), and has a calculated reversal potential of about −35 mV (Budde et al. 1997). According to the approximation of a Boltzmann distribution to the data points a fraction of 18% of I_h is activated at −71 mV (see Fig. 2*D*), carrying an inward current of −34 ± 2 pA (n = 28). Block of I_h shifted the resting membrane potential of TC neurons by −8 mV, a value in close agreement with previously reported hyperpolarization (−5 to −9 mV) in a number of different neuronal cell types (Day et al. 2005; Doan and Kunze 1999; Lupica et al. 2001; Maccaferri and McBain 1996).

Based on our results on rodent TC neurons (Meuth et al. 2003, 2006; Musset et al. 2006) and computer modeling (this study) it can be assumed that the classical K^+ leak current is roughly equally composed of pH-sensitive current through TASK3/TASK1 channels (I_{TASK}) and other pH-insensitive leak channels ($I_{K\text{-leak}}$). Although quantitative PCR experiments, subtype-specific modulation, and gene knock out point to a domination of TASK3 over TASK1, the $I_{K\text{-leak}}$ component may be carried by current through other members of the K_{2P} family. This conclusion is corroborated by the following findings. *1*) $I_{K\text{-leak}}$ revealing GHK rectification (Goldstein et al. 2001) is necessary to give closely matching modeling results. *2*) THIK, TRAAK, and TREK channels are expressed in dLGN, although a consignment to defined cell types is still missing. The functional expression of TREK and TRAAK (Patel and Lazdunski 2004) channels in TC neurons is in agreement with the presence of a leak current inhibited by cAMP and Ba^{2+} (Budde et al. 1997, 2005) and an I_{SO} component enhanced by arachidonic acid (Meuth et al. 2006). *3*) Modeling of the pH effect gives very similar results when both I_{TASK} and $I_{K\text{-leak}}$ are assumed to be pH sensitive.

It is noticeable that $HCN2^{-/-}$ mice show no plastic compensation for the loss of HCN2 channels. It has been noted before that, for example, cerebellar granule cells show a greater degree of plasticity in comparison with TC neurons in response

to TASK-1 deletion (Meuth et al. 2006). The reason for this difference is unknown.

Comparability between data obtained in vitro and in silico

The quantitative aspects of the complex relationship between current amplitudes in vitro, current amplitudes in the computer model, and their effect on the resting membrane potential depend on pharmacological tools, the large parameter space of the computer model, and experimental variations. Therefore it cannot be expected to achieve full match between experimental recordings and computer simulations. Still the following considerations reveal a reasonable degree of similarity between experiments and modeling. *1*) Injection of small depolarizing and hyperpolarizing current pulses (from resting membrane potential) to the model cell under current-clamp conditions resulted in 1- to 3-mV voltage deflections and allowed the calculation of the input resistance under control conditions (43 MΩ) and after the block of I_h (90 MΩ). Multiplying the difference in input resistance (47 MΩ) by the amplitude of I_h at the resting membrane potential of the model cell under control conditions (−130 pA) results in a voltage deflection of −6 mV. In whole cell recordings that typically reveal higher membrane resistances (some hundred megaohms) smaller currents (some tens of picoamperes) are able to induce similar voltage shifts. *2*) Absolute current values of I_h and I_{TASK} (amplitude of the pH-sensitive current in ZD7288) at −71 mV reveal very similar proportions in vitro ($I_h = 34 \pm 2$ pA, $n = 28$; $I_{TASK} = 31 \pm 2$ pA, $n = 25$) and in the computer model ($I_h = 131$ pA; $I_{TASK} = 137$ pA). Thus voltage changes induced by blocking/knocking out I_h in rats, mice, and the computer model ($V_{ZD} - V_R = -8$ mV; $V_{R/HCN2+/+} - V_{R/HCN2-/-} = -12$ mV; $V_3 - V_1 = -10$ mV; median = −10 mV) are in a range that has been described in several neuronal cell types (see above) and are comparable to the effects induced by blocking I_{TASK} ($V_R - V_{ZD/pH6.3} = 19$ mV; $V_{R/HCN2+/+} - V_{pH6.3/HCN-/-} = 11$ mV; $V_1 - V_{4/DC} = 13$ mV; median = 14 mV). *3*) The relationship between amplitudes measured in vitro (recording temperature ≈ 21°C) and the computer model (simulation temperature 35°C) is given by the Q_{10} value. Many enzyme reactions have a Q_{10} value near 3, as does the gating of many ion channels, including I_h (Hille 2001). Although values for absolute conductance of I_h seem to be <3 (Pena et al. 2006), the Q_{10} for I_h current amplitude in intracardiac neurons could be determined as 2.2 (Cuevas et al. 1997). Thus the amplitude of I_h at the resting membrane potential at 35°C can be expected to be −34 pA × 3.1 ($Q_{\Delta T}$ for a temperature difference of 14°C) = −105 pA, which is close to the −130 pA generated by the computer model. The temperature dependency of TASK channels is less clear because some K_{2P} channels reveal a sevenfold increase in current amplitude for a 10°C increment in temperature (Maingret et al. 2000).

Functional implications

The dorsal thalamus has a key role in regulating the flow of sensory information from the periphery to the primary sensory cortical areas and participates in the generation of thalamocortical oscillations associated with different states of consciousness and the status of absence epilepsy (Steriade et al. 1997). TC neurons are depolarized by neurotransmitters of the ascending brain stem system, including noradrenalin, serotonin, and acetylcholine (McCormick 1992). Whereas noradrenalin exerts this effect by the convergent modulation of $I_{K\text{-leak}}$ (i.e., closure) and I_h (i.e., depolarizing shift in activation), acetylcholine depolarizes TC neurons by closing TASK and I_{KIR} channels (Meuth et al. 2003). This depolarization is responsible for the transition of sleep-related rhythmic burst activity to tonic activity associated with periods of wakefulness and REM sleep.

The view that the counterbalancing actions of TASK and HCN on the resting membrane potential constitute a more general motive in the CNS is in agreement with the broad expression of HCN (Monteggia et al. 2000) and TASK (Talley et al. 2001) channels in the brain, the reciprocal modulation of I_h and I_{TASK} by serotonin and halothane on hypoglossal motoneurons (Sirois et al. 2002), and the analysis of dendritic excitability in mouse frontal cortex pyramidal cells (Day et al. 2005).

Pathophysiological implications

Neuronal activity leads to transient extracellular alkalinization followed by a persistent extracellular acidification (Chesler and Kaila 1992). In dLGN synchronous afferent activation, tonic activity, and rhythmic burst discharges induce extracellular and intracellular increases in H^+ concentrations (Meyer et al. 2000; Tong and Chesler 1999). The data presented here suggest that pH shifts induced by different forms of activity in dLGN should have rather small effects on the overall firing pattern and resting membrane potential. This is of special interest for periods of generalized absence epilepsy, where the highly synchronous burst pattern of large populations of TC neurons is not expected to be altered by pH changes arising from rhythmic activity.

Periods of brain ischemia are characterized by a decrease in extracellular pH to values as low as 6.0 (Siemkowicz and Hansen 1981; Simon et al. 1985). CNS neurons reveal extremely different sensitivity to ischemic insults (Centonze et al. 2001). The reason for this differential vulnerability is still largely unknown. Vulnerable neurons respond to ischemia with prolonged and strong membrane depolarization and subsequent cellular damage. Because of the joined modulation of TASK and HCN described here, it can be assumed that TC neurons show little depolarization in response to acidification during ischemic insults and thus a selective nonvulnerability. It seems, however, that other influences dominate the reaction of TC neurons to acute hypoxia (Erdemli and Crunelli 1998, 2000; Steinke et al. 1992; Szelies et al. 1991). Under these conditions there is an enhanced release of monoamines and nitric oxide—substances known to strongly activate I_h—in the thalamus. Therefore acute hypoxia leads to membrane depolarization and altered electrical properties of TC neurons and makes the dLGN a part of a system-preferential, topographically organized brain injury after ischemia (Erdemli and Crunelli 1998, 2000; Steinke et al. 1992; Szelies et al. 1991).

ACKNOWLEDGMENTS

Thanks to R. Ziegler and A. Jahn for excellent technical assistance.

GRANTS

This work was supported by Deutsche Forschungsgemeinschaft Grant BU 1019/5–2/7-1 (Leibniz-Program) to H.-C. Pape and Kommission Innovative Medizinische Forschung Grant BU 120501.

REFERENCES

Berg AP, Talley EM, Manger JP, and Bayliss DA. Motoneurons express heteromeric TWIK-related acid-sensitive K^+ (TASK) channels containing TASK-1 (KCNK3) and TASK-3 (KCNK9) subunits. *J Neurosci* 24: 6693–6702, 2004.

Budde T, Biella G, Munsch T, and Pape H-C. Lack of regulation by intracellular Ca^{2+} of the hyperpolarization-activated cation current in rat thalamic neurons. *J Physiol* 503.1: 79–85, 1997.

Budde T, Caputi L, Kanyshkova T, Staak R, Abrahamczik C, Munsch T, and Pape H-C. Impaired regulation of thalamic pacemaker channels through an imbalance of subunit expression in absence epilepsy. *J Neurosci* 25: 9871–9882, 2005.

Centonze D, Marfia GA, Pisani A, Picconi B, Giacomini P, Bernardi G, and Calabresi P. Ionic mechanisms underlying differential vulnerability to ischemia in striatal neurons. *Prog Neurobiol* 63: 687–696, 2001.

Chesler M and Kaila K. Modulation of pH by neuronal activity. *Trends Neurosci* 15: 396–402, 1992.

Craven KB and Zagotta WN. CNG and HCN channels: two peas, one pod. *Annu Rev Physiol* 68: 375–401, 2006.

Cuevas J, Harper AA, Trequattrini C, and Adams DJ. Passive and active membrane properties of isolated rat intracardiac neurons: regulation by H- and M-currents. *J Neurophysiol* 78: 1890–1902, 1997.

Czirjak G and Enyedi P. Formation of functional heterodimers between the TASK-1 and TASK-3 two-pore domain potassium channel subunits. *J Biol Chem* 277: 5426–5432, 2002.

Day M, Carr DB, Ulrich S, Ilijic E, Tkatch T, and Surmeier DJ. Dendritic excitability of mouse frontal cortex pyramidal neurons is shaped by the interaction among HCN, Kir2, and Kleak channels. *J Neurosci* 25: 8776–8787, 2005.

Doan TN and Kunze DL. Contribution of the hyperpolarization-activated current to the resting membrane potential of rat nodose sensory neurons. *J Physiol* 514: 125–138, 1999.

Duprat F, Lesage F, Fink M, Reyes R, Heurteaux C, and Lazdunski M. TASK, a human background K^+ channel to sense external pH variations near physiological pH. *EMBO J* 16: 5464–5471, 1997.

Erdemli G and Crunelli V. Response of thalamocortical neurons to hypoxia: a whole-cell patch-clamp study. *J Neurosci* 18: 5212–5224, 1998.

Erdemli G and Crunelli V. Release of monoamines and nitric oxide is involved in the modulation of hyperpolarization-activated inward current during acute thalamic hypoxia. *Neuroscience* 96: 565–574, 2000.

Franz O, Liss B, Neu A, and Roeper J. Single-cell mRNA expression of HCN1 correlates with a fast gating phenotype of hyperpolarization-activated cyclic nucleotide-gated ion channels (Ih) in central neurons. *Eur J Neurosci* 12: 2685–2693, 2000.

Goldstein SA, Bockenhauer D, O'Kelly I, and Zilberberg N. Potassium leak channels and the KCNK family of two-P-domain subunits. *Nat Rev Neurosci* 2: 175–184, 2001.

Hille B. *Ion Channels of Excitable Membranes.* Sunderland, MA: Sinauer, 2001.

Hines ML and Carnevale NT. NEURON: a tool for neuroscientists. *Neuroscientist* 7: 123–135, 2001.

Huguenard JR and McCormick DA. Simulation of the currents involved in rhythmic oscillations in thalamic relay neurons. *J Neurophysiol* 68: 1373–1383, 1992.

Jones EG and Hendry SH. Differential Calcium Binding Protein Immunoreactivity Distinguishes Classes of Relay Neurons in Monkey Thalamic Nuclei. *Eur J Neurosci* 1: 222–246, 1989.

Jones SW. On the resting potential of isolated frog sympathetic neurons. *Neuron* 3: 153–161, 1989.

Kaila K and Ransom BR. *pH and Brain Function.* New York: Wiley–Liss, 1998.

Kim Y, Bang H, and Kim D. TASK-3, a new member of the tandem pore K(+) channel family. *J Biol Chem* 275: 9340–9347, 2000.

Lesage F. Pharmacology of neuronal background potassium channels. *Neuropharmacology* 44: 1–7, 2003.

Ludwig A, Budde T, Stieber J, Moosmang S, Wahl C, Holthoff K, Langebartels A, Wotjak C, Munsch T, Zong X, Feil S, Feil R, Lancel M, Chien KR, Konnerth A, Pape H-C, Biel M, and Hofmann F. Absence epilepsy and sinus dysrhythmia in mice lacking the pacemaker channel HCN2. *EMBO J* 22: 216–224, 2003.

Lupica CR, Bell JA, Hoffman AF, and Watson PL. Contribution of the hyperpolarization-activated current (*I*(h)) to membrane potential and GABA release in hippocampal interneurons. *J Neurophysiol* 86: 261–268, 2001.

Maccaferri G and McBain CJ. The hyperpolarization-activated current (Ih) and its contribution to pacemaker activity in rat CA1 hippocampal stratum oriens-alveus interneurones. *J Physiol* 497. 1: 119–130, 1996.

Maingret F, Lauritzen I, Patel AJ, Heurteaux C, Reyes R, Lesage F, Lazdunski M, and Honore E. TREK-1 is a heat-activated background K(+) channel. *EMBO J* 19: 2483–2491, 2000.

Malcolm AT, Kourennyi DE, and Barnes S. Protons and calcium alter gating of the hyperpolarization-activated cation current (I_h) in rod photoreceptors. *Biochem Biophys Acta* 1609: 183–192, 2003.

McCormick DA. Neurotransmitter actions in the thalamus and cerebral cortex and their role in neuromodulation of thalamocortical activity. *Prog Neurobiol* 39: 337–388, 1992.

McCormick DA and Huguenard JR. A model of the electrophysiological properties of thalamocortical relay neurons. *J Neurophysiol* 68: 1384–1400, 1992.

McCormick DA and Pape H-C. Properties of a hyperpolarization-activated cation current and its role in rhythmic oscillation in thalamic relay neurones. *J Physiol* 431: 291–318, 1990.

Meuth P, Meuth SG, Jacobi D, Broicher T, Pape H-C, and Budde T. Get the Rhythm: modeling of neuronal activity. *JUNE Fall 2005* 4: A1–A11, 2005.

Meuth SG, Aller MI, Munsch T, Schuhmacher T, Seidenbecher T, Kleinschnitz C, Pape H-C, Wiendl H, Wisden W, and Budde T. The contribution of TASK-1-containing channels to the function of dorsal lateral geniculate thalamocortical relay neurons. *Mol Pharmacol* 69: 1468–1476, 2006.

Meuth SG, Budde T, Kanyshkova T, Broicher T, Munsch T, and Pape H-C. Contribution of TWIK-related acid-sensitive K^+ channel 1 (TASK1) and TASK3 channels to the control of activity modes in thalamocortical neurons. *J Neurosci* 23: 6460–6469, 2003.

Meuth SG, Kanyshkova T, Landgraf P, Pape H-C, and Budde T. Influence of Ca^{2+}-binding proteins and the cytoskeleton on Ca^{2+}-dependent inactivation of high-voltage activated Ca^{2+} currents in thalamocortical relay neurons. *Pfluegers Arch* 450: 111–122, 2005.

Meyer TM, Munsch T, and Pape H-C.. Activity-related changes in intracellular pH in rat thalamic relay neurons. *Neuroreport* 11: 33–37, 2000.

Millar JA, Barratt L, Southan AP, Page KM, Fyffe RE, Robertson B, and Mathie A. A functional role for the two-pore domain potassium channel TASK-1 in cerebellar granule neurons. *Proc Natl Acad Sci USA* 97: 3614–3618, 2000.

Monteggia LM, Eisch AJ, Tang MD, Kaczmarek LK, and Nestler EJ. Cloning and localization of the hyperpolarization-activated cyclic nucleotide-gated channel family in rat brain. *Brain Res Mol Brain Res* 81: 129–139, 2000.

Munsch T and Pape H-C. Modulation of the hyperpolarization-activated cation current of rat thalamic relay neurones by intracellular pH. *J Physiol* 519: 493–504, 1999.

Musset B, Meuth SG, Liu GX, Derst C, Wegner S, Pape H-C, Budde T, Preisig-Muller R, and Daut J. Effects of divalent cations and spermine on the K^+ channel TASK-3 and on the outward current in thalamic neurons. *J Physiol* 572: 639–657, 2006.

Pape H-C. Queer current and pacemaker: the hyperpolarization-activated cation current in neurons. *Annu Rev Physiol* 58: 299–327, 1996.

Pape H-C, Budde T, Mager R, and Kisvarday Z. Prevention of Ca^{2+}-mediated action potentials in GABAergic local circuit neurons of the thalamus by a transient K^+ current. *J Physiol* 478: 403–422, 1994.

Patel AJ and Lazdunski M. The 2P-domain K^+ channels: role in apoptosis and tumorigenesis. *Pfluegers Arch* 448: 261–273, 2004.

Pena F, Amuzescu B, Neaga E, and Flonta ML. Thermodynamic properties of hyperpolarization-activated current (*Ih*) in a subgroup of primary sensory neurons. *Exp Brain Res* May 5, 2006, published online. DOI: 10.1007/s00221-006-0473-z.

Porcello DM, Smith SD, and Huguenard JR. Actions of U-92032, a T-type Ca^{2+} channel antagonist, support a functional linkage between I_T and slow intrathalamic rhythms. *J Neurophysiol* 89: 177–185, 2003.

Rajan S, Wischmeyer E, Liu GX, Preisig-Muller R, Daut J, Karschin A, and Derst C. TASK-3, a novel tandem pore domain acid-sensitive K^+ channel. An extracellular histidine as pH sensor. *J Biol Chem* 275: 16650–16657, 2000.

Sieg F, Obst K, Gorba T, Riederer B, Pape H-C, and Wahle P. Postnatal expression pattern of calcium-binding proteins in organotypic thalamic cultures and in the dorsal thalamus in vivo. *Brain Res Dev Brain Res* 110: 83–95, 1998.

Siemkowicz E and Hansen AJ. Brain extracellular ion composition and EEG activity following 10 minutes ischemia in normo- and hyperglycemic rats. *Stroke* 12: 236–240, 1981.

Simon RP, Benowitz N, Hedlund R, and Copeland J. Influence of the blood-brain pH gradient on brain phenobarbital uptake during status epilepticus. *J Pharmacol Exp Ther* 234: 830–835, 1985.

Sirois JE, Lynch C 3rd, and Bayliss DA. Convergent and reciprocal modulation of a leak K^+ current and I_h by an inhalational anaesthetic and neurotransmitters in rat brainstem motoneurones. *J Physiol* 541: 717–729, 2002.

Steinke W, Sacco RL, Mohr JP, Foulkes MA, Tatemichi TK, Wolf PA, Price TR, and Hier DB. Thalamic stroke. Presentation and prognosis of infarcts and hemorrhages. *Arch Neurol* 49: 703–710, 1992.

Steriade M, Jones EG, and McCormick DA. *Thalamus.* Amsterdam: Elsevier, 1997.

Stevens DR, Seifert R, Bufe B, Muller F, Kremmer E, Gauss R, Meyerhof W, Kaupp UB, and Lindemann B. Hyperpolarization-activated channels HCN1 and HCN4 mediate responses to sour stimuli. *Nature* 413: 631–635, 2001.

Szelies B, Herholz K, Pawlik G, Karbe H, Hebold I, and Heiss WD. Widespread functional effects of discrete thalamic infarction. *Arch Neurol* 48: 178–182, 1991.

Talley EM, Solorzano G, Lei Q, Kim D, and Bayliss DA. CNS distribution of members of the two-pore-domain (KCNK) potassium channel family. *J Neurosci* 21: 7491–7505, 2001.

Tong CK and Chesler M. Activity-evoked extracellular pH shifts in slices of rat dorsal lateral geniculate nucleus. *Brain Res* 815: 373–381, 1999.

Watkins CS and Mathie A. A non-inactivating K^+ current sensitive to muscarinic receptor activation in rat cultured cerebellar granule neurons. *J Physiol* 491: 401–412, 1996.

Williams SR, Turner JP, Hughes SW, and Crunelli V. On the nature of anomalous rectification in thalamocortical neurones of the cat ventrobasal thalamus in vitro. *J Physiol* 505: 727–747, 1997.

Zhan XJ, Cox CL, Rinzel J, and Sherman SM. Current-clamp and modeling studies of low-threshold calcium spikes in cells of the cat's lateral geniculate nucleus. *J Neurophysiol* 81: 2360–2373, 1999.

Zong X, Stieber J, Ludwig A, Hofmann F, and Biel M. A single histidine residue determines the pH sensitivity of the pacemaker channel HCN2. *J Biol Chem* 276: 6313–6319, 2001.